Electronic Supplementary Material (ESI) for ChemComm.

Ruthenium-catalyzed aerobic oxidative decarboxylation of amino acids: a green, zero-waste route to biobased nitriles**

Laurens Claes, Jasper Verduyckt, Ivo Stassen, Bert Lagrain and Dirk E. De Vos*

Supporting Information

Table of content

1. GENERAL INFORMATION

All chemicals were purchased and used without further purification. Ru^0/Al_2O_3 and Ru^0/C, both containing 5 wt% of Ru, were obtained from Alfa Aesar and Johnson Matthey respectively. Other ruthenium-based catalysts were prepared from ruthenium (III) chloride hydrate (Acros Organics, 35-40% Ru) and ruthenium (III) acetylacetonate (ABCR, 99%). γ-Alumina (Sigma-Aldrich), zirconium (IV) oxide (Alfa Aesar), anatase (Sigma-Aldrich), cerium (IV) oxide (Alfa Aesar, 99.5%), cobalt (II,III) oxide (Acros Organics) and sodium hydroxide (Fischer Scientific, 99.1%) were used in the preparation of heterogeneous catalysts. In the oxidative decarboxylation L-alanine (Janssen, 99%), L-aspartic acid monosodium salt (Sigma Aldrich, ≥ 98%), L-glutamic acid monosodium salt hydrate (Sigma-Aldrich, ≥ 99%), DL-homoserine (Sigma-Aldrich, 99%), L-isoleucine (Fluka, ≥ 99.0%), L-leucine (Acros, 99%), D-norleucine (Sigma-Aldrich) and L-valine (Acros, 99%) were used as reagents; *n*-pentylamine (Sigma-Aldrich, 99%) was used as a model reactant for amine oxidation. Reactions were performed in deionized water; methanol-d_4 (Sigma-Aldrich, 99.8 atom% D) was used as deuterated solvent for NMR analysis.

2. GENERAL PROCEDURES

2.1 Material synthesis

2.1.1 Catalysts

A powdered support (2.0 g) was suspended in an aqueous solution of $RuCl_3.3H_2O$ (0.13 g, 60 mL) and stirred vigorously for 15 min at room temperature. Afterwards, the pH was adjusted to 13.2 by the addition of an aqueous NaOH solution (2 M), and the suspension was stirred for 24 h. The supported ruthenium hydroxide catalyst, denoted as $Ru(OH)_x$/support, was recovered by centrifugation, washed several times with deionized water and freeze-dried.[S1]

The hydroxyapatite-supported ruthenium catalyst was also synthesized through ion-exchange of calcium with ruthenium.[S2] Therefore, a suspension of hydroxyapatite (2 g) in a solution of $RuCl_3.3H_2O$ (0.1055 g) in deionized water (100 mL) was stirred for 24 h at room temperature. The solid material was recovered by centrifugation, washed several times with deionized water and freeze-dried.

2.1.2 Catalyst supports

The hydrotalcite support was prepared by co-precipitation from the corresponding metal nitrate salts in alkaline medium under ambient conditions. $Mg(NO_3)_2.6H_2O$ (17.95 g) and $Al(NO_3)_3.9H_2O$ (11.25 g) were dissolved in deionized water (100 mL). This aqueous solution was added dropwise by using a Braun Perfusor Space pump to deionized water (100 mL) at pH 10 under magnetic stirring. The pH was kept constant during the synthesis by the addition of an aqueous solution of Na_2CO_3 (2 M). Afterwards, the aqueous suspension was stirred at room temperature for 24 h. The white precipitate was recovered by centrifugation, washed several times with deionized water, and freeze-dried.

The hydroxyapatite support was prepared according to the method reported by Ishikawa *et al.* (1990).[S3] A solution of $(NH_4)_2HPO_4$ (7.92 g) in deionized water (250 mL) was brought at pH 12 by the addition of aqueous ammonia (100 mL). This solution was added dropwise and under constant mixing to another solution containing $Ca(NO_3)_2.4H_2O$ (23.60 g) in deionized water (150 mL). The suspension was heated under reflux for 4 h, and the white precipitate was recovered by filtration afterwards. The hydroxyapatite material was dried overnight at 353 K, and calcined for 30 min (973 K, 3 K min^{-1}).

The other materials, γ-Al_2O_3, ZrO_2, TiO_2, CeO_2 and Co_3O_4, were obtained commercially.

2.2 Catalyst characterization

X-ray diffraction (PXRD) measurements were performed on a STOE StadiP diffractometer with Cu Kα radiation. Scanning electron microscopy (SEM) was carried out on a Philips XL 30 FEG microscope after coating the samples with Au. Nitrogen physisorption measurements were performed on a Micromeritics 3Flex surface analyzer at 77 K. Prior to the measurement, the samples were outgassed at 423 K for 6 h under vacuum. The ruthenium content was determined via inductively coupled plasma atomic emission spectroscopy (ICP-AES) using a Jobin Yvon Ultima spectrometer; ruthenium was detected at 267.876 nm. Therefore, the material (50 mg) was degraded by heating at 383 K in *aqua regia* (HNO_3/HCl = 1:3 v/v; 0.5 mL) and HF (3 mL) for 1 h. After cooling to room temperature, deionized water (10 mL) and H_3BO_3 (2.8 g) were added and the mixture was further diluted to a final volume of 100 mL.

2.3 Typical reaction procedure

A stainless steel reactor (internal volume: 11 mL) was loaded with an aqueous solution of the amino acid (0.1 M, 0.2 mmol), $Ru(OH)_x$/support (5 mol% Ru) and a magnetic stirring bar. The reactor was sealed and an oxygen pressure of 30 bar was applied. The suspension was heated to 373 K and stirred for 24 h. Afterwards, methanol-d_4 (0.5 mL) was added to the reactor to obtain a homogeneous reaction mixture. The solid catalyst was separated from the suspension by centrifugation.

2.4 Product analysis and identification

Reaction mixtures were analyzed by ^{1}H-NMR in order to determine the conversion and selectivity in the oxidative decarboxylation reaction. ^{1}H-NMR spectra were recorded on a Bruker Avance 400 MHz spectrometer equipped with a BBI 5 mm probe. The broad signal due to the presence of water was suppressed by applying an adapted pulse program: p1 8 µs; pl1 -1 db; pl9 50 db; o1P on the resonance signal of water, determined from the previous ^{1}H-NMR measurement: ds 2; ns 32; d1 5 s; aq 2.55 s; sw 16. In addition, products were identified by gas chromatography coupled to mass spectrometry (GC-MS) with an Agilent 6890 GC, equipped with a HP-5ms column, coupled to a 5973 MSD mass spectrometer.

3. RESULTS

3.1 Catalyst characterization

The ruthenium-based catalysts were characterized by powder X-ray diffraction and elemental analysis. The highly active $Ru(OH)_x/\gamma\text{-}Al_2O_3$ catalyst was also characterized by SEM-EDX and nitrogen physisorption.

3.1.1 Powder X-ray diffraction (PXRD)

The diffraction patterns show that the structure of the support is hardly affected upon immobilization of ruthenium by precipitation-deposition in highly alkaline conditions (Figure S1-Figure S6).

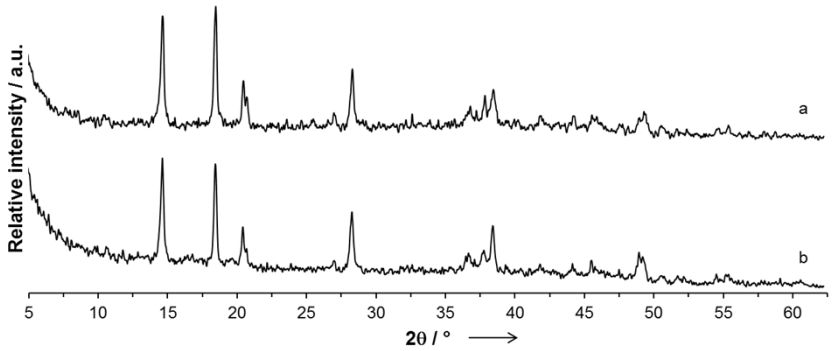

Figure S1. Powder X-ray diffraction patterns: (a) $\gamma\text{-}Al_2O_3$, (b) $Ru(OH)_x/\gamma\text{-}Al_2O_3$.

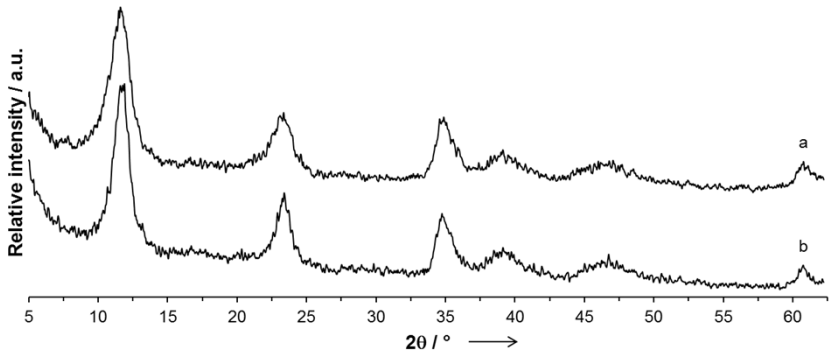

Figure S2. Powder X-ray diffraction patterns: (a) hydrotalcite, (b) $Ru(OH)_x$/hydrotalcite.

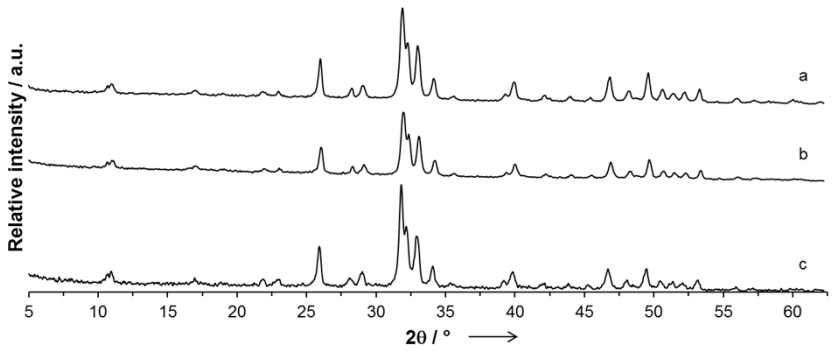

Figure S3. Powder X-ray diffraction patterns: (a) hydroxyapatite, (b) Ru^{n+}/hydroxyapatite and (c) $Ru(OH)_x$/hydroxyapatite.

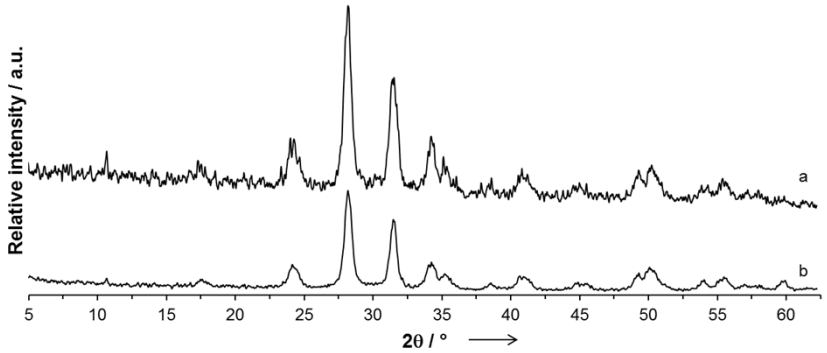

Figure S4. Powder X-ray diffraction patterns: (a) ZrO_2, (b) $Ru(OH)_x/ZrO_2$.

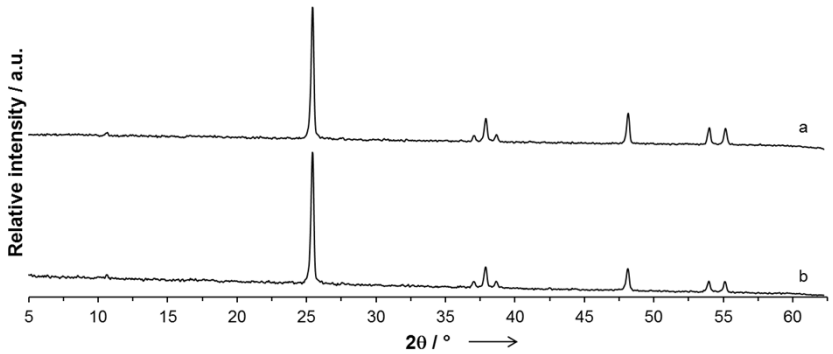

Figure S5. Powder X-ray diffraction patterns: (a) TiO_2 (anatase), (b) $Ru(OH)_x/TiO_2$ (anatase).

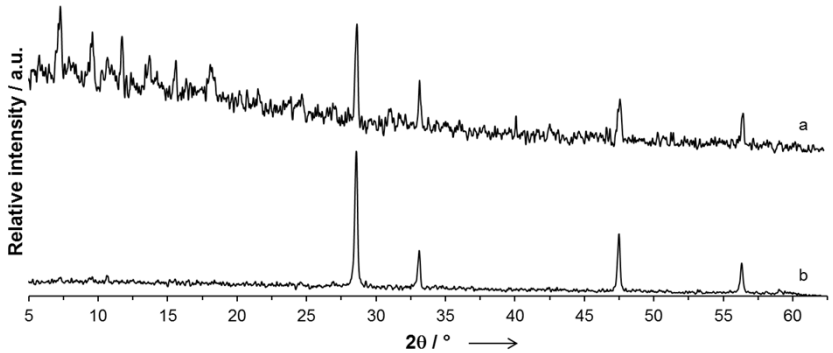

Figure S6. Powder X-ray diffraction patterns: (a) CeO_2, (b) $Ru(OH)_x/CeO_2$.

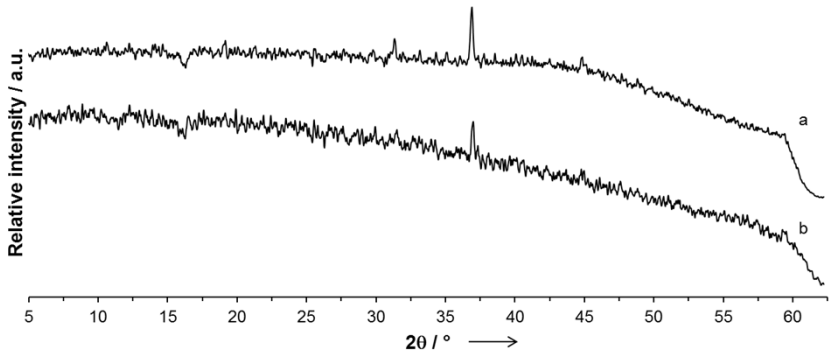

Figure S7. Powder X-ray diffraction patterns: (a) Co_3O_4, (b) $Ru(OH)_x/Co_3O_4$.

3.1.2 Scanning electron microscopy (SEM) and energy-dispersive X-ray spectroscopy (EDX)

The $Ru(OH)_x/\gamma$-Al_2O_3 material consists of large particles, with dimensions in the µm range, as observed from the SEM micrograph (Figure S8). In addition, EDX analysis of several distinct particles shows that ruthenium is distributed rather heterogeneously on the outer surface. On average, the Ru-content was determined at 3.61 wt%; this result provides complementary information to bulk elemental analysis (Table S2). A typical EDX spectrum also shows the presence of Al and O near the surface (Figure S9).

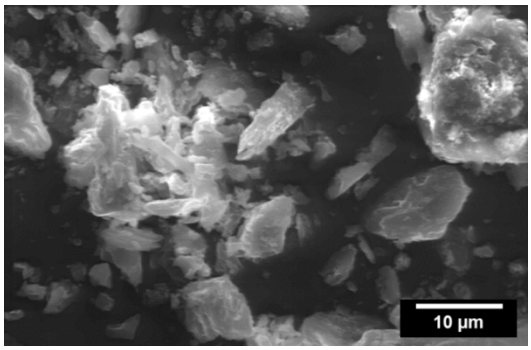

Figure S8. SEM micrograph of the $Ru(OH)_x/\gamma$-Al_2O_3 catalyst.

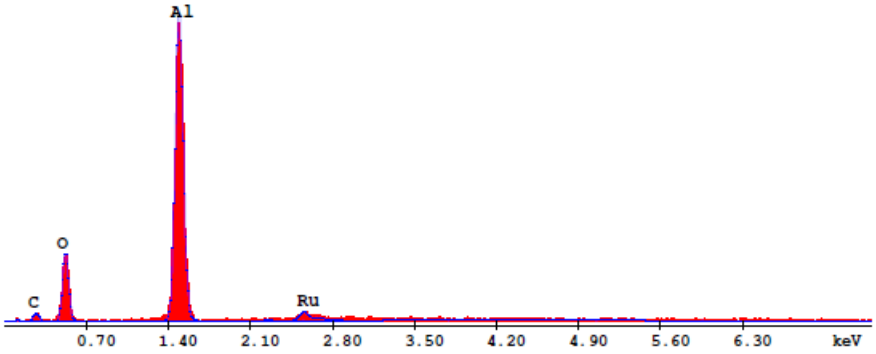

Figure S9. EDX spectrum of the $Ru(OH)_x/\gamma$-Al_2O_3 catalyst.

3.1.3 Nitrogen physisorption

The textural properties of the $Ru(OH)_x/\gamma$-Al_2O_3 catalyst were determined from nitrogen physisorption measurements at 77 K (Figure S10, Table S1). The adsorption-desorption isotherm shows type IV-behavior, which is typical for mesoporous materials. The BET surface area of this material was determined at 152 $m^2\ g^{-1}$; this is considerably higher than for other supported ruthenium catalysts, for instance the materials prepared from CeO_2 or TiO_2 supports, which have a surface area below 10 $m^2\ g^{-1}$.

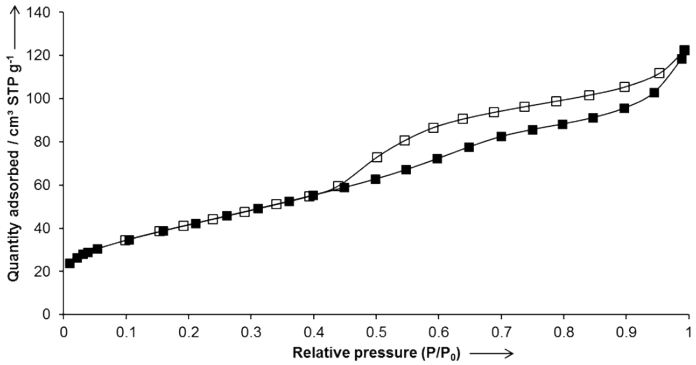

Figure S10. Nitrogen physisorption isotherm, at 77 K, for the $Ru(OH)_x/\gamma$-Al_2O_3 catalyst (●: closed symbols, adsorption; open symbols, desorption).

Table S1. Textural properties of γ-Al_2O_3 and the as-synthesized $Ru(OH)_x/\gamma$-Al_2O_3 catalyst.

Material	S[a] [m^2 g^{-1}]	V[b] [cm^3 g^{-1}]	D[c] [nm]
γ-Al_2O_3	139 ± 1	0.18	5 ± 2
$Ru(OH)_x/\gamma$-Al_2O_3	152 ± 1	0.18	5 ± 2

[a] BET surface area. [b] Barrett-Joyner-Halenda (BJH) pore volume. [c] BJH average pore diameter.

3.1.4 Bulk elemental analysis (ICP-AES)

The protocol for the synthesis of supported ruthenium catalysts aimed at a metal loading of 2 wt%. The actual ruthenium content, determined by elemental analysis (ICP-AES), varies between 1.7 and 2.8 wt% and is shown in Table S2. The Ca/P-ratio of the hydroxyapatite support was determined at 1.58, which is comparable with the theoretical ratio of 1.67 ($Ca_{10}(PO_4)_6(OH)_2$).

Table S2. Ruthenium content of the as-synthesized catalysts.

Catalyst	Ru content [wt%]
$Ru(OH)_x/\gamma$-Al_2O_3	2.32
Ru^{n+}/hydroxyapatite[a]	1.71
$Ru(OH)_x$/hydroxyapatite	2.76
$Ru(OH)_x/ZrO_2$	2.31
$Ru(OH)_x$/hydrotalcite	2.79
$Ru(OH)_x/TiO_2$ (anatase)	1.99
$Ru(OH)_x/CeO_2$	2.58
$Ru(OH)_x/Co_3O_4$	2.44

[a] Immobilization through ion-exchange of calcium with ruthenium.

3.1.5 Acid-base characterization

The acid-base properties of the Ru-containing materials and their supports were estimated by measuring the pH of an aqueous suspension (Table S3). This accurately reflects the effect that these materials will have on the pH of a reaction in a fully aqueous medium. For the most active catalysts (**a**-**i**), the pH varies between 6.5 and 9, whereas the suspensions of TiO_2-, CeO_2- and Co_3O_4-supported catalysts (**j**-**o**) have a pH > 9. A mild basicity in the catalytic system thus seems beneficial for catalysis (compare with the data in Table 1 of the main manuscript).

Table S3. Acid-base properties of the Ru-based catalysts and their precursors.

	Material	pH[a]		Material	pH[a]
a	γ-Al_2O_3	8.98	**j**	TiO_2 (anatase)	7.11
b	$Ru(OH)_x/\gamma$-Al_2O_3	8.52	**k**	$Ru(OH)_x/TiO_2$ (anatase)	9.80
c	Hydroxyapatite	7.51	**l**	CeO_2	7.08
d	Ru^{n+}/hydroxyapatite[b]	6.55	**m**	$Ru(OH)_x/CeO_2$	9.16
e	$Ru(OH)_x$/hydroxyapatite	8.40	**n**	Co_3O_4	10.29
f	ZrO_2	7.71	**o**	$Ru(OH)_x/Co_3O_4$	9.27
g	$Ru(OH)_x/ZrO_2$	8.05			
h	Hydrotalcite	9.20			
i	$Ru(OH)_x$/hydrotalcite	9.05			

[a] pH of a suspension containing 45 mg solid material in 3 mL deionized H_2O after overnight stirring. [b] Immobilization through ion-exchange of calcium with ruthenium.

3.2 Optimization of reaction conditions

The catalytic performance was evaluated as a function of oxygen pressure, amount of catalyst and temperature.

3.2.1 Oxygen pressure

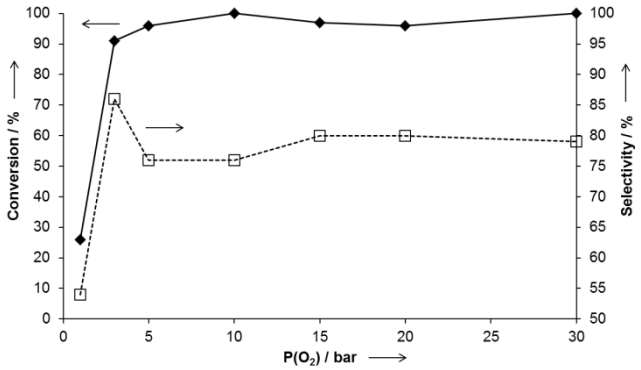

Figure S11. Ru-catalyzed oxidative decarboxylation of leucine at various oxygen pressures. Conditions: L-leucine (0.2 mmol), $Ru(OH)_x/\gamma$-Al_2O_3 (5 mol% Ru), H_2O (2 mL), 100°C, 24 h.

3.2.2 Catalyst/amino acid ratio

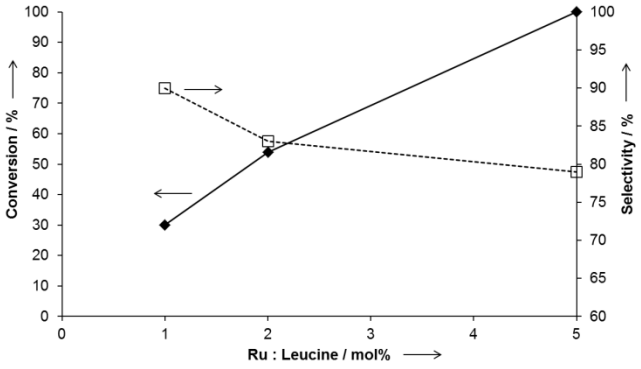

Figure S12. Ru-catalyzed oxidative decarboxylation of leucine at various Ru/leucine ratios. Conditions: L-leucine (0.2 mmol), $Ru(OH)_x/\gamma$-Al_2O_3, H_2O (2 mL), O_2 (30 bar), 100°C, 24 h.

3.2.3 Temperature

At 110°C a similar yield of 79% (95% conversion; 83% selectivity) is already obtained within 6 h. The reaction was not optimized further in terms of temperature.

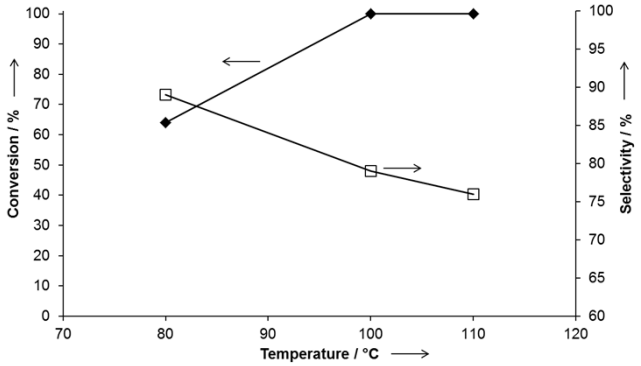

Figure S13. Ru-catalyzed oxidative decarboxylation of leucine at various temperatures. Conditions: L-leucine (0.2 mmol), $Ru(OH)_x/\gamma$-Al_2O_3 (5 mol% Ru), H_2O (2 mL), O_2 (30 bar), 24 h.

3.3 Catalyst recycling

A filtration test was performed during the oxidative decarboxylation of glutamic acid in water (Figure S14). The $Ru(OH)_x/\gamma$-Al_2O_3 catalyst was separated by filtration from the reaction mixture after 2 h, when the conversion was at 11%. The reaction proceeded further in the residual reaction mixture until a final conversion of 79% was reached after 24 h, whereas no significant increase in conversion has been detected in the filtrate.

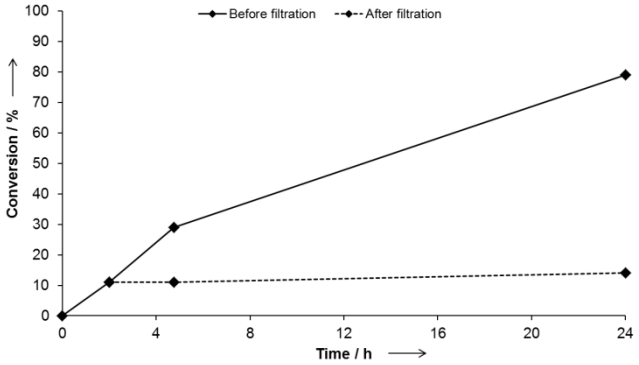

Figure S14. Ru-catalyzed oxidative decarboxylation of sodium glutamate with catalyst separation after 2 h. Conditions: L-glutamic acid monosodium salt (0.6 mmol), $Ru(OH)_x/\gamma$-Al_2O_3 (5 mol% Ru), H_2O (6 mL), O_2 (30 bar), 100°C.

The stability of the heterogeneous catalyst was evaluated by reusing the spent catalyst in several reaction cycles (Table S4). Although the conversion of leucine decreased in consecutive cycles, ICP-AES analyses showed that < 2% of the total amount of immobilized Ru was leached from the solid material into the aqueous solution. Therefore, the decrease in catalytic activity cannot be the result of Ru leaching.

Table S4. Recycling of the $Ru(OH)_x/\gamma$-Al_2O_3 catalyst for the oxidative decarboxylation of leucine.[a]

Run	Conversion of leucine [%]	Selectivity to isovaleronitrile [%]
1	> 99	78
2	75	88
3	50	82

[a] Conditions: L-leucine (0.2 mmol), $Ru(OH)_x/\gamma$-Al_2O_3 (5 mol% Ru), H_2O (2 mL), O_2 (30 bar), 24 h. The catalyst was washed with NaOH (1 M, 5 mL), deionized water (2 x 10 mL) and acetone (10 mL) and afterwards dried overnight at 60°C.

3.4 Oxidation of primary amines *vs.* oxidative decarboxylation of amino acids

The $Ru(OH)_x/\gamma\text{-}Al_2O_3$ catalyst was evaluated for the oxidation of *n*-pentylamine (Figure S15) and the oxidative decarboxylation of leucine (Figure S16). The catalyst is far more active for amine oxidation than for amino acid oxidative decarboxylation. Nevertheless, for both types of substrates, the nitrile is obtained as the major product, but the selectivity is decreased upon prolonged reaction times by the consecutive hydration into an amide.

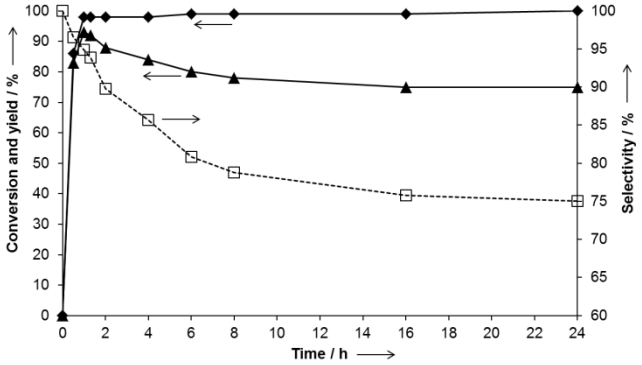

Figure S15. Ru-catalyzed aerobic oxidation of *n*-pentylamine. Conditions: *n*-pentylamine (0.2 mmol), $Ru(OH)_x/\gamma\text{-}Al_2O_3$ (5 mol% Ru), H_2O (2 mL), O_2 (30 bar). Legend: conversion of *n*-pentylamine (🕘), yield of valeronitrile (□) and selectivity to valeronitrile (○).

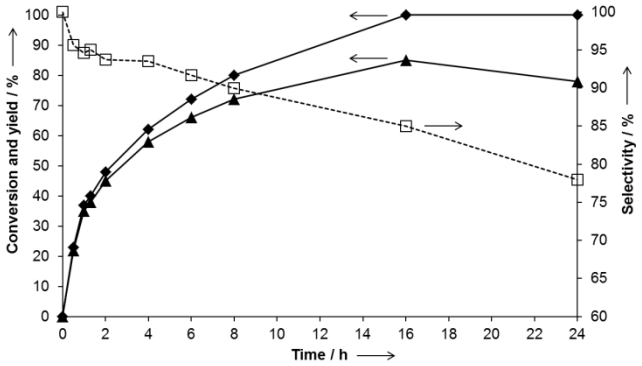

Figure S16. Ru-catalyzed aerobic oxidative decarboxylation of leucine. Conditions: L-leucine (0.2 mmol), $Ru(OH)_x/\gamma\text{-}Al_2O_3$ (5 mol% Ru), H_2O (2 mL), O_2 (30 bar). Legend: conversion of leucine (🕘), yield of isovaleronitrile (□) and selectivity to isovaleronitrile (○).

The origin of nitrile hydration was elucidated in an additional set of experiments, using valeronitrile as the substrate instead of *n*-pentylamine or leucine (Table S5). Ruthenium itself appears to be the actual catalyst for this side reaction.

Table S5. Hydration of valeronitrile to valeramide.[a]

	Catalyst	Conversion [%]	Selectivity [%]
1	-	5	> 99
2	$\gamma\text{-}Al_2O_3$	< 1	-
3	$\gamma\text{-}Al_2O_3$[b]	< 1	-
4	Hydrotalcite	< 1	-
5	Hydrotalcite[b]	3	> 99
6	$RuCl_3$	41	> 99
7	$Ru(OH)_x/\gamma\text{-}Al_2O_3$	37	> 99

[a] Conditions: valeronitrile (0.2 mmol), catalyst (5 mol% Ru or 45 mg support), H_2O (2 mL), O_2 (30 bar), 24 h. Reaction at pH 7. [b] After pretreatment with NaOH.

3.5 Product identification

Isovaleronitrile or 3-methyl-butyronitrile (1b, MW = 83)

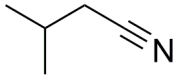

^{1}H NMR (400 MHz, CD_3OD/H_2O): δ = 2.40 (d, ^{3}J(H,H) = 6.26 Hz, 2H; -CH-C**H**$_2$-CN), 2.02 (m, ^{3}J(H,H) = 6.65 Hz, 1H; $(CH_3)_2$>C**H**-CH_2-), 1.03 ppm (d, ^{3}J(H,H) = 6.67 Hz, 6H; ($C\underline{H}_3)_2$>CH-);

^{13}C NMR (300 MHz, CD_3OD/H_2O): δ = 122.7 (1C; -CH_2-**C**N), 26.7-26.5 (2C; $(CH_3)_2$>**C**H-**C**H_2-CN), 22.4 ppm (2C; -CH<(**C**$H_3)_2$);

GC/MS (EI, 70 eV): *m/z* (rel. int., %): 83 (0.2) [M^+], 82 (2) [M^+-H], 68 (7) [M^+-CH_3], 52 (5), 43 (100) [$C_3H_7^+$], 42 (7), 41 (75) [M^+-C_3H_6], 40 (14), 39 (40), 38 (10), 37 (6).

Acetonitrile (2b, MW = 41)

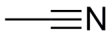

^{1}H NMR (400 MHz, CD_3OD/H_2O): δ = 2.08 ppm (s, 3H; C**H**$_3$-CN);

^{13}C NMR (300 MHz, CD_3OD/H_2O): δ = 118.2 (1C; CH_3-**C**N), 0.1 ppm (1C; **C**H_3-CN);

GC/MS (EI, 70 eV): *m/z* (rel. int., %): 42 (3) [$(M+1)^+$], 41 (100) [M^+], 40 (66) [M^+-H], 39 (23), 38 (15).

Isobutyronitrile or 2-methyl-propionitrile (3b, MW = 69)

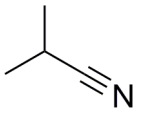

^{1}H NMR (400 MHz, CD_3OD/H_2O): δ = 2.86 (sep, ^{3}J(H,H) = 7.05 Hz, 1H; $(CH_3)_2$>C**H**-CN), 1.30 ppm (d, ^{3}J(H,H) = 7.05 Hz, 6H; ($C\underline{H}_3)_2$>CH-);

^{13}C NMR (300 MHz, CD_3OD/H_2O): δ = 127.1 (1C; >CH-**C**N), 20.3 (2C; -CH<(**C**$H_3)_2$), 20.2 ppm (1C; $(CH_3)_2$>**C**H-CN);

GC/MS (EI, 70 eV): *m/z* (rel. int., %): 69 (3) [M^+], 68 (54) [M^+-H], 54 (25) [M^+-CH_3], 53 (10), 52 (12), 51 (7), 42 (100) [M^+-HCN], 41 (26) [$C_3H_5^+$], 40 (6), 39 (13), 38 (5).

(*S*)-2-Methyl-butyronitrile (4b, MW = 83)

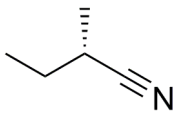

^{1}H NMR (400 MHz, CD_3OD/H_2O): δ = 2.75 (m, ^{3}J(H,H) = 7.09 Hz, 1H; (CH_3)(-CH_2-)>C**H**-CN), 1.63 (m, ^{3}J(H,H) = 7.39 Hz, 2H; CH_3-C**H**$_2$-CH-), 1.29 (d, ^{3}J(H,H) = 7.12 Hz, 3H; C**H**$_3$-CH-), 1.04 ppm (t, ^{3}J(H,H) = 7.45 Hz, 3H; C**H**$_3$-CH_2-);

^{13}C NMR (300 MHz, CD_3OD/H_2O): δ = 124.9 (1C; -CH_2-**C**N), 26.6 (1C; >CH-**C**H_2-CH_3), 26.4 (1C; -CH_2-**C**H(-CH_3)-CN), 16.5 (1C; >CH-**C**H_3), 10.6 ppm (1C; -CH_2-**C**H_3);

GC/MS (EI, 70 eV): *m/z* (rel. int., %): 83 (0.1) [M^+], 82 (2) [M^+-H], 68 (2) [M^+-CH_3], 56 (5) [M^+-HCN], 55 (100) [M^+-C_2H_4], 54 (54) [$C_3H_4N^+$], 53 (5), 52 (9), 51 (6), 41 (10), 39 (15).

Valeronitrile or pentanenitrile (5b, MW = 83)

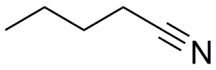

^{1}H NMR (400 MHz, CD_3OD/H_2O): δ = 2.48 (t, ^3J(H,H) = 7.01 Hz, 2H; -CH_2-C**H**$_2$-CN), 1.64 (quin, ^3J(H,H) = 7.30 Hz, 2H; -CH_2-C**H**$_2$-CH_2-), 1.45 (sex, ^3J(H,H) = 7.40 Hz, 2H; CH_3-C**H**$_2$-CH_2-), 0.93 ppm (t, ^3J(H,H) = 7.44 Hz, 3H; C**H**$_3$-CH_2-);

^{13}C NMR (300 MHz, CD_3OD/H_2O): δ = 121.9 (1C; -CH_2-**C**N), 26.5 (1C; -CH_2-**C**H_2-CH_2), 21.2 (1C; -**C**H_2-CH_3), 15.8 (1C; -**C**H_2-CN), 12.4 ppm (1C; -CH_2-**C**H_3);

GC/MS (EI, 70 eV): *m/z* (rel. int., %): 83 (0.2) [M^+], 82 (4) [M^+-H], 55 (24), 54 (63) [M^+-C_2H_5], 52 (7), 51 (5), 43 (90) [$C_3H_7^+$], 42 (6), 41 (100) [M^+-C_3H_6], 40 (9), 39 (27).

3-Cyano-propanoic acid (6b, MW = 99)

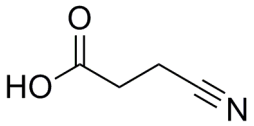

^{1}H NMR (400 MHz, CD_3OD/H_2O): δ = 2.64 (t, ^3J(H,H) = 7.04 Hz, 2H; -CH_2-C**H**$_2$-CN), 2.50 ppm (t, ^3J(H,H) = 6.66 Hz, 2H; -CH_2-C**H**$_2$-C(=O)-O^-Na^+);

^{13}C NMR (300 MHz, CD_3OD/H_2O): δ = 178.4 (1C; -CH_2-**C**OO^-Na^+), 121.6 (1C; -CH_2-**C**N), 32.4 (1C; -CH_2-**C**H_2-C(=O)-O^-Na^+), 13.8 ppm (1C; -CH_2-**C**H_2-CN);

GC/MS (EI, 70 eV): *m/z* (rel. int., %): 99 (28) [M^+], 98 (1) [M^+-H], 82 (10) [M^+-OH], 56 (13), 55 (23), 54 (100) [M^+-COOH], 53 (7), 52 (14), 51 (8), 45 (22) [$COOH^+$], 42 (5).

3-Cyano-propanoic acid (7b, MW = 85)

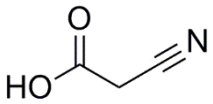

^{1}H NMR (400 MHz, CD_3OD/H_2O): δ = 3.45 ppm (s, 2H; HOOC-C**H**$_2$-CN);

^{13}C NMR (300 MHz, CD_3OD/H_2O): δ = 169.6 (1C; -CH_2-**C**OO^-Na^+), 117.8 (1C; -CH_2-**C**N), 26.6 (1C; NC-**C**H_2-C(=O)-O^-Na^+), 13.8 ppm (1C; -CH_2-**C**H_2-CN).

3-Hydroxy-propionitrile (8b, MW = 71)

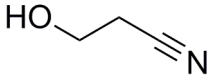

^{1}H NMR (400 MHz, CD_3OD/H_2O): δ = 3.82 (t, ^3J(H,H) = 5.96 Hz, 2H; HO-C**H**$_2$-CH_2-), 2.71 ppm (t, ^3J(H,H) = 5.86 Hz, 2H; -CH_2-C**H**$_2$-CN);

^{13}C NMR (300 MHz, CD_3OD/H_2O): δ = 120.3 (1C; -CH_2-**C**N), 57.1 (1C; -CH_2-**C**H_2OH), 21.0 ppm (1C; $HOCH_2$-**C**H_2-CN);

GC/MS (EI, 70 eV): *m/z* (rel. int., %): 53 (6) [M^+-H_2O], 52 (9), 42 (15), 41 (100) [$C_2H_3N^+$], 40 (16), 39 (8), 38 (11), 31 (97) [CH_3O^+].

4. REFERENCES

[S1] K. Yamaguchi and N. Mizuno, *Angew. Chem. Int. Ed.*, 2003, **42**, 1480

[S2] K. Yamaguchi, K. Mori, T. Mizugaki, K. Ebitani, K. Kaneda, *J. Am. Chem. Soc.*, 2000, **122**, 7144.

[S3] K. Ishikawa, M. Kon, S. Tenshin, N. Kuwayama, *Dent. Mater. J.*, 1990, **9**, 58.